Design of tuned mass dampers incorporating wire rope springs: Part I: Dynamic representation of wire rope springs

Rafik R. Gerges*, Barry J. Vickery

Alan G. Davenport Wind Engineering Group, Department of Civil and Environmental Engineering, Faculty of Engineering Science, The University of Western Ontario, London, Ontario, Canada N6A 5B9

Abstract

Two mathematical models for describing the effective stiffness and the equivalent viscous damping ratio of wire rope springs, as amplitude dependent, were developed. Twenty-four springs were tested in free vibration and the displacement decays were recorded. The free vibration time history was used to calculate the effective stiffness and the equivalent viscous damping ratio. For each displacement amplitude, the effective stiffness was determined from the observed period of vibration. The equivalent viscous damping ratio was determined from the logarithmic decrement of the velocity between the points of zero potential energy. The proposed models are semi-empirical in nature and require no testing since all parameters are fully determined from the physical properties of springs.
© 2005 Elsevier Ltd. All rights reserved.

Keywords: Damping; Energy dissipation; Experimental; Friction; Modeling; Non-linear; Stiffness; System identification; Wire rope

1. Introduction

Tuned mass dampers are auxiliary systems incorporated into structures to reduce their resonant response under dynamic forces. A tuned mass damper consists of a mass, a spring and a damper. The spring and the damper components can be implemented in a number of ways. Possessing elastic and energy dissipation characteristics, the wire rope spring combines the spring and the damper actions in one device. Both the stiffness and the damping of the wire rope spring can be adjusted by varying wire rope diameter, wire rope structure, wire material, coil diameter, number of coils and/or spring orientation.

While significant advances have been made in the modelling of wire rope springs, experimental work is still needed to calibrate the available models [1–13]. Therefore, considerable experience is necessary for the designer to decide on the spring dimensions before testing. Usually, a number of different springs are selected for testing before one specific configuration is chosen. Such exploration procedures do not allow fine-tuning of the spring dynamic characteristics to the requirements of the particular application at hand. Moreover, the available models, to be incorporated in the analysis of structural systems, require incremental non-linear time domain analysis.

Linearisation often results in an accurate representation of the characteristics of many non-linear dynamic systems. The non-linear stiffness of the wire rope spring can be approximated by an effective spring constant that maintains the same natural frequency at a certain displacement amplitude. The complicated energy dissipation mechanism can be represented by an equivalent viscous damping mechanism that, for a given amplitude, dissipates the same amount of energy.

This paper describes a large set of dynamic tests that were conducted to quantify the amplitude-dependent effective stiffness and equivalent viscous damping ratio of the wire rope springs in the tension–compression mode of deformation. Twenty-four wire rope springs were

* Corresponding address: Nabih Youssef & Associates Structural Engineers, 800 Wilshire Boulevard, Suite 200, Los Angeles, CA, USA. Tel.: +1 213 362 0707; fax: +1 213 688 3018.
E-mail addresses: rgerges@nyase.com, rafik_gerges@yahoo.ca (R.R. Gerges).

tested in free vibration and the displacement decays were recorded. For each recorded displacement amplitude, the effective stiffness was determined from the observed period of vibration. The equivalent viscous damping ratio was determined from the logarithmic decrement of the velocity between the points of zero potential energy.

Two mathematical models that describe the effective stiffness and the equivalent viscous damping ratio, as amplitude-dependent quantities, were developed. For each wire rope spring, the effective stiffness values were normalised by their minimum value and the displacement amplitude values were normalised by the amplitude value corresponding to the minimum effective stiffness. The normalisation process resulted in similar trends for the stiffness–amplitude and the damping–amplitude relationships for all the springs tested. The minimum effective stiffness was related to the stiffness of a ring beam subjected to a point load and the corresponding displacement amplitude was related to the dimensions of the wire rope spring. The normalised effective stiffness was fitted with two polynomials, which are functions of the normalised displacement amplitude. On the basis of an understanding of the actual energy dissipation mechanism, the equivalent viscous damping ratio was also described as a function of the normalised displacement amplitude.

2. Experimental study

2.1. Wire rope springs

Twenty-four wire rope springs were fabricated for the intended experimental study. Fig. 1 shows a schematic drawing of a wire rope spring. The wire rope diameter, d_r, and the coil diameter, D_c, were varied as listed in Table 1. The wire rope structure is 6×19 with an independent wire rope core (IWRC) for diameters 25.40 and 12.70 mm and is 7×19 with a wire strand core (WSC) for diameters 7.938, 6.350 and 3.175 mm. To compare with other wire rope structures, one spring was made of a 7×7 WSC wire rope of 1.587 mm diameter. The ratio D_c/d_r was chosen to be in the range of 10–25 (with one exception of 33) as listed in Table 1. The spring was intended to be two half-circles on both sides of the aluminium retainers. However, after being fabricated, it took a near elliptical shape with the major axis, D_{c1}, as the distance between the two retainers and the minor axis, D_{c2}, perpendicular to the retainers (see Table 1). D_c was calculated as the average of D_{c1} and D_{c2}. Fig. 2 shows some of the springs used in this study.

2.2. Test set-up and procedures

Each wire rope spring was placed between a moving pendulum and a reaction column as shown in Fig. 3. The pendulum was pushed manually for several cycles to build up motion and then was released to vibrate freely. The displacements, x, at the wire rope spring attachment point
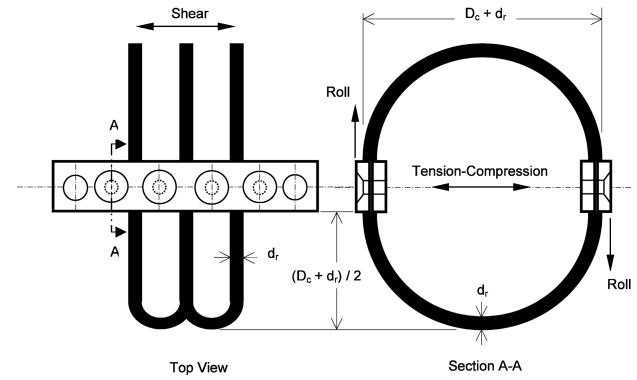

Fig. 1. A Schematic drawing of a wire rope spring.

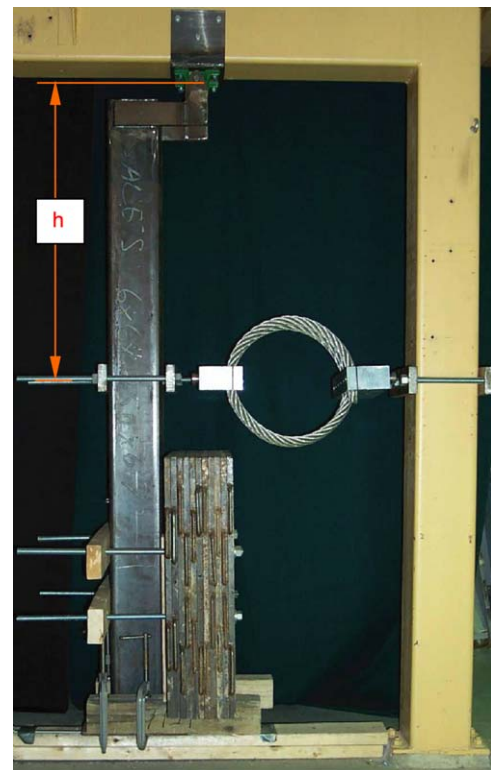Fig. 2. A photograph of some of the wire rope springs tested.

Fig. 3. A photograph of the pendulum set-up.

were recorded. A typical filtered displacement, x, time history is shown in Fig. 4.

Table 1
Dimensions and properties of wire rope springs

#	d_r (mm)	D_{c1} (mm)	D_{c2} (mm)	D_{c1}/D_{c2} ratio	D_c (mm)	D_c/d_r ratio	k^{ns}/k^{min} ratio	k^{ps}/k^{min} ratio	k^{fs}/k^{min} ratio	X_r^{min} cal./test
1	25.40	664	613	1.08	639	25.14	135	9.7	0.93	0.95
2	25.40	422	403	1.05	413	16.24	140	10.0	0.96	0.84
3	25.40	322	286	1.13	304	11.97	170	12.2	1.18	0.93
4	12.70	329	314	1.05	322	25.32	133	9.3	0.92	1.07
5	12.70	285	273	1.04	279	21.97	149	10.3	1.03	1.00
6	12.70	246	239	1.03	243	19.10	159	11.0	1.10	1.01
7	12.70	220	211	1.04	216	16.97	158	11.0	1.10	1.07
8	12.70	197	184	1.07	191	15.00	172	12.0	1.19	0.96
9	12.70	173	163	1.06	168	13.23	170	11.8	1.18	1.00
10	12.70	157	143	1.10	150	11.81	157	10.9	1.13	1.04
11	12.70	163	140	1.16	152	11.97	131	9.1	0.98	1.09
12	12.70	160	140	1.14	150	11.81	143	9.9	1.03	1.07
13	12.70	154	144	1.07	149	11.73	174	12.1	1.20	0.93
14	12.70	138	128	1.08	133	10.47	164	11.4	1.13	0.88
15	7.938	155	145	1.07	150	18.90	118	9	0.92	1.03
16	7.938	154	145	1.07	150	18.90	114	8.6	0.88	0.94
17	7.938	157	142	1.11	150	18.90	118	8.9	0.91	1.08
18	6.350	163	156	1.05	160	25.12	119	9.0	0.90	1.00
19	6.350	112	109	1.03	111	17.40	141	10.7	1.07	1.01
20	6.350	62	60	1.03	61	9.61	135	10.2	1.02	0.96
21	3.175	83	79	1.05	81	25.51	138	10.4	1.02	1.20
22	3.175	56	55	1.02	56	17.48	134	10.2	1.00	1.15
23	3.175	32	31	1.03	32	9.92	141	10.6	1.04	0.90
24[a]	1.587	53	51	1.05	52	33	61	10.1	0.69	1.43

Shaded rows represent springs used for verification of mathematical models.

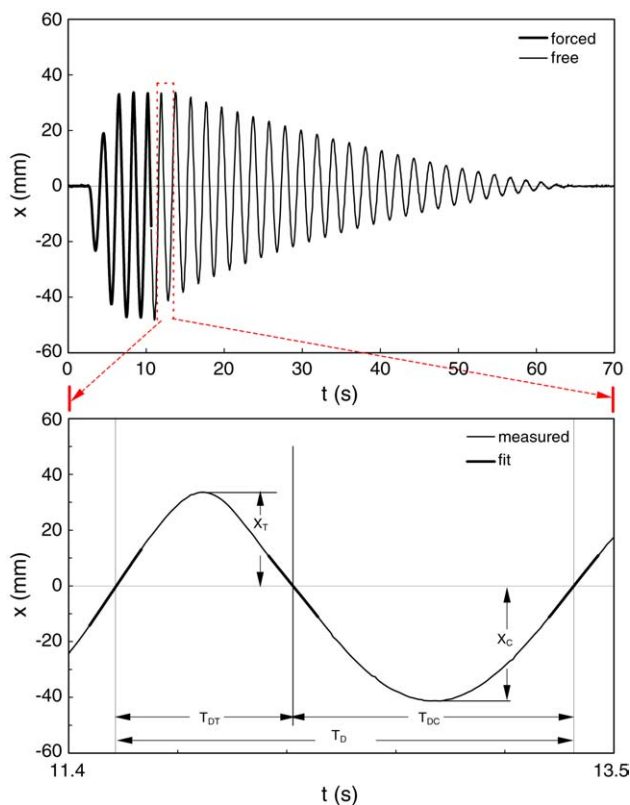[a] Wire rope structure 7×7.

Fig. 4. A typical displacement time history.

2.3. Pendulum rotational stiffness

The rotational stiffness of the pendulum, k_p^θ, for small rotations, is

$$k_p^\theta = m_p a_g z \tag{1}$$

where m_p is the mass of the pendulum, a_g is the acceleration due to gravity and z is the distance between the pivot and the pendulum centre of mass. The spring stiffness to pendulum stiffness ratio was chosen to maintain a balance between two sources of error. These were errors associated with the calculation of the wire rope spring stiffness and errors due to interpolation of stiffness and damping between recorded amplitudes.

3. Analysis procedures

3.1. Representative amplitude, X_r

Since the force–displacement relationship is asymmetrical as shown in Fig. 5, the free vibration tension amplitude, X_T, and compression amplitude, X_C, differ considerably within the same vibration cycle as shown in Fig. 4. A representative amplitude, X_r, was chosen as
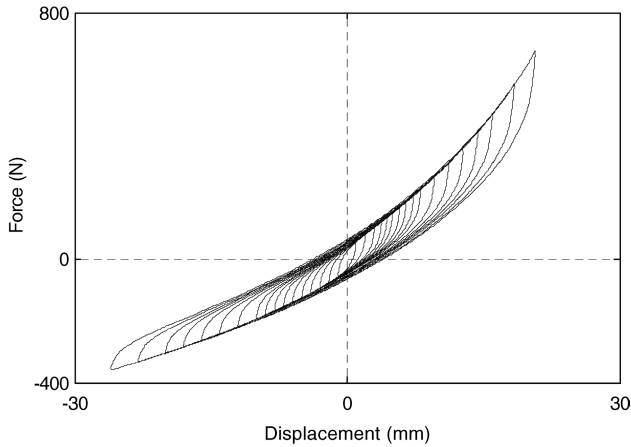
$$X_r = \sqrt{X_T X_C}. \tag{2}$$

Fig. 5. A typical force–displacement relationship for the tension–compression mode of deformation.

3.2. Amplitude-dependent effective stiffness, k_{wr}

The damped periods of the vibration, T_D, were obtained from the free vibration time history (see Fig. 4). The effective stiffness, k_{wr}, corresponding to a particular representative displacement amplitude, X_r, was determined to produce the same natural frequency as the non-linear spring. This equivalence criterion was adopted because the natural frequency of the tuned mass damper strongly influences its effectiveness.

The calculation procedures, for each X_r, are as follows:

1. The circular natural damped frequency of the rotational single-degree-of-freedom, SDOF, system is given by

$$\omega_D = \frac{2\pi}{T_D}. \tag{3}$$

2. The total rotational stiffness of the SDOF system is given by

$$k_t^\theta = \frac{\omega_D^2 I_p}{(1 - \beta^2)} \tag{4}$$

where I_p is the mass moment of inertia of the pendulum about the pivot and β is the equivalent viscous damping ratio of the SDOF system evaluated in the next section

3. The spring rotational stiffness is given by

$$k_{wr}^\theta = k_t^\theta - k_p^\theta \tag{5}$$

4. The tension–compression stiffness per coil of the wire rope spring is given by

$$k_{wr} = \frac{k_{wr}^\theta}{n_c h^2} \tag{6}$$

where n_c is the number of coils.

3.3. Amplitude-dependent equivalent viscous damping ratio, β_{wr}

Damping in structures is usually represented by an equivalent viscous damping. It is the simplest form of

damping to use since the governing differential equation of motion is linear. The commonest method for defining the equivalent viscous damping is equating the energy dissipated over a vibration cycle by the actual damping mechanism to that dissipated by a viscous damping mechanism [14].

The energy dissipated in a free vibration cycle by a rotational SDOF with viscous damping is given by

$$E_D^{fV} = 2 I_p \omega_n \beta \int_0^{\frac{2\pi}{\omega_D}} \dot{\theta}(t)^2 \, dt \tag{7}$$

where the rotation is described by

$$\theta(t) = \exp(-\beta \omega_n t) \left(C_{\theta 1} \cos \left(\omega_n \sqrt{1 - \beta^2} t \right) \right.$$
$$\left. + C_{\theta 2} \sin \left(\omega_n \sqrt{1 - \beta^2} t \right) \right) \tag{8}$$

and the rotational velocity is

$$\dot{\theta}(t) = \frac{d\theta(t)}{dt}. \tag{9}$$

The initial conditions are defined as

$$\theta(0) = 0 \tag{10a}$$

and

$$\dot{\theta}(0) = \dot{\theta}_0. \tag{10b}$$

The initial conditions are used to determine the constants $C_{\theta 1}$ and $C_{\theta 2}$ in Eq. (8). An expression for the dissipated energy per cycle in free vibration for a viscously damped SDOF was obtained by performing the integral in Eq. (7) and is given by

$$E_D^{fV} = \frac{1}{2} I_p \dot{\theta}_0^2 \left(1 - \exp \left(\frac{-4\pi\beta}{\sqrt{1 - \beta^2}} \right) \right). \tag{11}$$

Regardless of the actual damping mechanism, the energy dissipation between points of zero potential energy can be expressed in terms of the change in the kinetic energy as

$$E_D^f = \frac{1}{2} I_p \left(\dot{\theta}_0^2 - \dot{\theta}_1^2 \right). \tag{12}$$

By equating E_D^{fV} to E_D^f, an expression for the equivalent viscous damping ratio is obtained as

$$\beta = \frac{\frac{\delta}{2\pi}}{\sqrt{1 + \left(\frac{\delta}{2\pi} \right)^2}} \tag{13a}$$

where

$$\delta = \ln \left(\frac{\dot{\theta}_0}{\dot{\theta}_1} \right). \tag{13b}$$

For a spring, which has a hysteretic force–displacement relationship, zero displacement corresponds to a value for the force (see Fig. 5) and therefore there is some potential

energy stored in the spring. The zero-potential-energy condition is satisfied only at points of zero acceleration. The displacement time history was numerically differentiated twice to determine points of zero acceleration. Velocities corresponding to zero accelerations $\dot{\theta}_0$ and $\dot{\theta}_1$ were used in Eq. (13) to obtain the equivalent viscous damping ratio. Since the pendulum motion was recorded in terms of displacement at the spring level, the rotational velocity, $\dot{\theta}$, for small rotations, can be related to the translational velocity, $\dot{x}$, by

$$\dot{\theta} \cong \frac{\dot{x}}{h}. \tag{14}$$

The only component that dissipates a significant amount of energy in the rotational SDOF system is the wire rope spring. The equivalent viscous damping ratio, calculated according to the above-mentioned procedures, should be corrected for the ratio of the total system stiffness to the spring stiffness. The energy dissipated by a rotational SDOF system with viscous damping in one cycle of harmonic vibration is

$$E_D^{hV} = 2\pi\beta\frac{\omega}{\omega_n}k_t^\theta\Theta^2 \tag{15}$$

where ω is the frequency of response and Θ is the amplitude of rotation. Since the response of a system is most sensitive to damping when vibrating at its natural frequency, the damping equivalence point is always chosen at $\omega = \omega_n$. If the stiffness is provided only by the wire rope spring, k_{wr}^θ, then the corresponding equivalent viscous damping ratio, β_{wr}, is given by

$$\beta_{wr} = \frac{k_t^\theta}{k_{wr}^\theta}\beta. \tag{16}$$

3.4. Dynamic properties based on the half-cycle

Considering tension and compression separately, the half-cycle period is T_{DT} or T_{DC} and the corresponding amplitude is X_T or X_C, respectively, as shown in Fig. 4. The velocities $\dot{\theta}_0$ and $\dot{\theta}_1$ are calculated for the half-cycle under consideration. To carry out the analysis for the half-cycles, Eq. (3) is replaced by

$$\omega_D = \frac{2\pi}{2\,T_{DT}} \tag{17a}$$

for the tension half-cycle or

$$\omega_D = \frac{2\pi}{2\,T_{DC}} \tag{17b}$$

for the compression half-cycle. Also, Eq. (13b) should be replaced by

$$\delta = 2\log_e\left(\frac{\dot{\theta}_0}{\dot{\theta}_1}\right). \tag{18}$$

4. Experimental results and modelling

4.1. Effective stiffness, k_{wr}

4.1.1. Typical stiffness–amplitude relationship

A typical effective stiffness based on full vibration cycles versus the representative amplitude, X_r, is shown in Fig. 6. It also shows the effective stiffness based on tension and compression half-cycles. For the stiffness based on full cycles, it decreases rapidly with the increase of X_r up to a certain point where it reaches its minimum value, $k^{\min}$ at amplitude $X_r^{\min}$, after which k_{wr} slightly increases with the increase of X_r. The rapid decrease of k_{wr} with X_r increase could be attributed to the increase of slip between individual wires, therefore reducing the wire rope's effective moment of inertia. In the small amplitude range, the non-linear geometric effects do not play a noticeable role and hence the effective stiffnesses based on full cycles, tension half-cycles and compression half-cycles are all equal. This agrees with the recorded symmetric hysteresis loops under small amplitudes (see Fig. 5). As the amplitude increases, stiffening takes place on the tension side while softening is experienced on the compression side. The full cycle effective stiffness represents the average.

4.1.2. Minimum effective stiffness, $k^{\min}$, and corresponding amplitude, $X_r^{\min}$

The minimum value for the effective stiffness based on the full vibration cycle, $k^{\min}$, and the corresponding representative amplitude, $X_r^{\min}$, were obtained from experimental results for all the 24 springs and are listed in Table 1.

On the basis of the energy method and considering only the bending deformations, an expression for the tension–compression stiffness of a ring beam subject to a point load was obtained as [15]

$$k_r = \frac{E\,I_{xx}}{D_c^3}\frac{8}{\left(\frac{\pi}{4} - \frac{2}{\pi}\right)} \tag{19}$$

where I_{xx} is the cross section moment of inertia about the axis of bending and E is the modulus of elasticity. Three different values were assigned to I_{xx}, based on: a no-slip condition; partial slip between strands but no-slip between individual wires within the same strand; and a full slip condition. The corresponding stiffness values were k^{ns}, k^{ps} and k^{fs}, respectively. k^{ns}, k^{ps} and k^{fs} were normalised by $k^{\min}$ and are given in Table 1. The ratios $k^{fs}/k^{\min}$ for springs 1–23 are all in the near vicinity of unity which suggests that $k^{\min}$ can be accurately predicted using Eq. (19) with a full slip condition considered in calculating I_{xx}.

To predict the representative displacement amplitude corresponding to $k^{\min}$, an empirical expression in the form

$$X_r^{\min} = 0.086\frac{D_c^{1.24}}{d_r^{0.24}} \tag{20}$$

best fits the experimentally obtained $X_r^{\min}$ values (see Table 1).
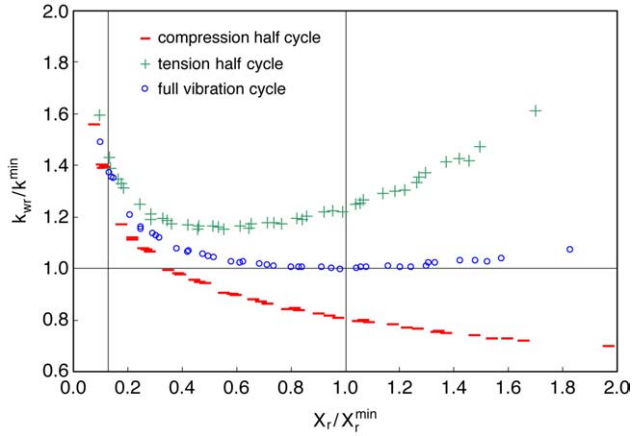
Fig. 6. A typical normalised effective stiffness versus normalised displacement amplitude.
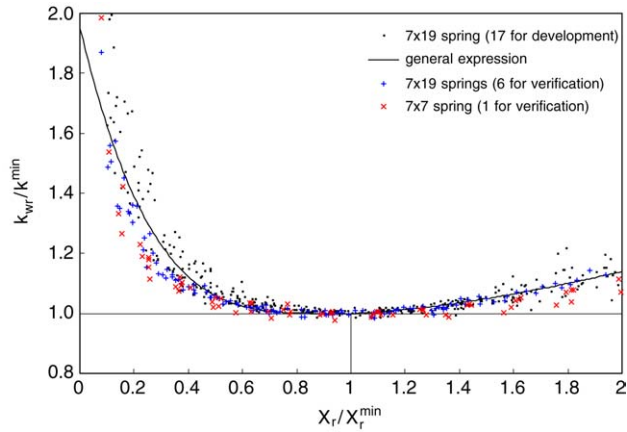

Fig. 7. Normalised effective stiffness versus normalised displacement amplitude for all springs.

4.1.3. General expression for the amplitude-dependent effective stiffness, $k_{wr}(X_r)$

For each spring, the effective stiffness values, k_{wr}, and the representative amplitude values, X_r, were normalised by $k^{\min}$ and $X_r^{\min}$, respectively. The normalisation process was repeated for the 24 springs and normalised values are plotted in Fig. 7. A general expression for the amplitude-dependent effective stiffness was obtained, through fitting, as

$$k_{wr}(X_r) = k^{\min}\left(1 + 0.95\left(1 - \frac{X_r}{X_r^{\min}}\right)^4\right)$$
$$\text{for} \quad X_r \leq X_r^{\min} \tag{21a}$$

and

$$k_{wr}(X_r) = k^{\min}\left(1 + 0.14\left(\frac{X_r}{X_r^{\min}} - 1\right)^{1.5}\right)$$
$$\text{for} \quad X_r > X_r^{\min} \tag{21b}$$

and is plotted in Fig. 7.
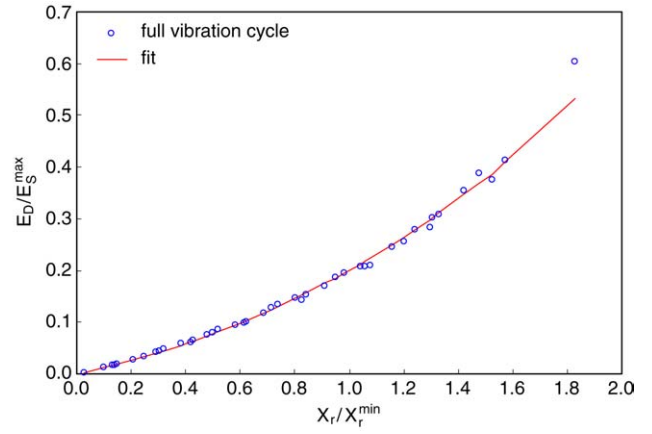

Fig. 8. A typical normalised energy dissipation versus normalised displacement amplitude.

4.2. Equivalent viscous damping ratio, β_{wr}

4.2.1. Damping mechanisms

To identify the energy dissipation mechanism, a typical energy dissipation/amplitude relationship is plotted in Fig. 8. The energy dissipated is normalised by the maximum strain energy that can be stored in the wire rope spring, which is

$$E_S^{\max} = \frac{1}{2}\left\{k_{wr}\left(2X_r^{\min}\right)\right\}2X_r^{\min}. \tag{22}$$

The relationship between the energy dissipation and the amplitude suggested a fit in the form

$$E_D^f = C_{ED1}X_r + C_{ED2}X_r^2, \tag{23}$$

which represents the combination of two mechanisms. The term proportional to the amplitude represents a friction damping mechanism as shown in Fig. 9(a). The term proportional to the amplitude squared represents a rate-independent linear damping [14,16] in which the damping force is proportional to displacement as shown in Fig. 9(b). η is a dimensionless damping constant. A condition for achieving slip is

$$k_{wr}(X_r) \; X_r \geq F_f + \frac{\pi \eta k_{wr} X_r}{2} \tag{24}$$

and was considered in fitting the dissipated energy with Eq. (23).

4.2.2. General expression for the amplitude-dependent damping ratio, $\beta_{wr}(X_r)$

The equivalent viscous damping ratio values, β_{wr}, were plotted versus the normalised displacement amplitude values, $X_r/X_r^{\min}$, for the 24 springs and are shown in Fig. 10. The relationship between the viscous damping ratio equivalent to the combined damping mechanism and the amplitude needs to be described. When the energy dissipated by a viscous damping mechanism under harmonic excitation
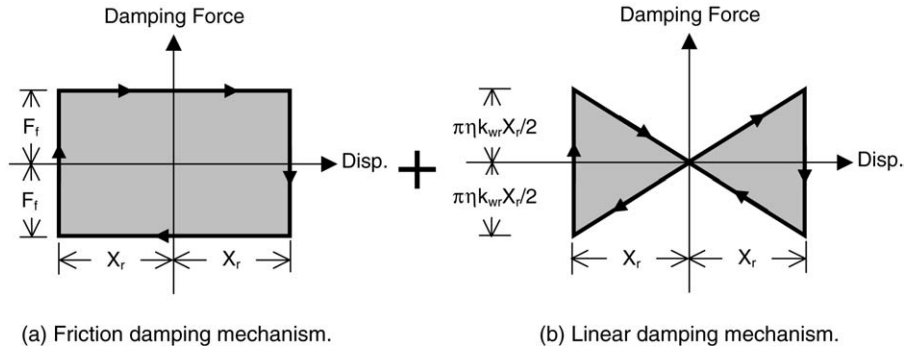
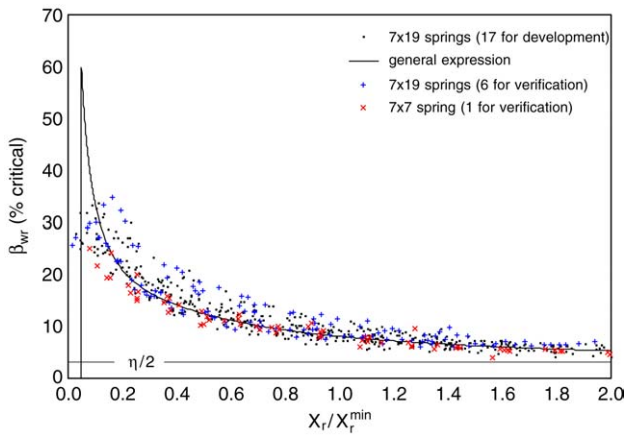Fig. 9. Combined damping mechanism of wire rope springs.

Fig. 10. Equivalent viscous damping ratio versus normalised displacement amplitude for all springs.

is equated to that dissipated by both the friction and linear damping mechanisms as

$$2\pi\beta_{wr}\frac{\omega}{\omega_n}k_{wr}X_r^2 = 4F_f X_r + \pi\eta k_{wr}X_r^2, \tag{25}$$

a relationship between β_{wr} and X_r, for $\omega = \omega_n$, is obtained as

$$\beta_{wr}(X_r) = \frac{2}{\pi}\frac{F_f}{k_{wr}X_r} + \frac{\eta}{2}. \tag{26}$$

By fitting the expression given by Eq. (26) and fulfilling the slip condition given by Eq. (24), values for the non-dimensional parameters $F_f/(k^{\min}X_r^{\min})$ and η are obtained as 0.0776 and 0.0627, respectively, and the fitted expression is shown in Fig. 10. As X_r increases, the contribution of the friction damping to β_{wr} decreases. For large X_r values, β_{wr} approaches a value of $\eta/2$ (see Fig. 10).

4.3. Applicability to other wire rope structures

The effective stiffness and equivalent viscous damping ratio expressions were developed on the basis of springs having wire rope structures of 7×19 WRS or 6×19 IWRC.

The spring made of wire rope structure 7×7 is shown to match the trend of the above-mentioned data (see Figs. 7 and 10). However, discrepancies are observed between measured and predicted $X_r^{\min}$ and $k^{\min}$ for the 7×7 spring. Further testing is required to check the applicability of the models developed to other wire rope structures.

5. Conclusions

The effective stiffness decreases as the vibration amplitude increases up to its minimum value, beyond which the stiffness slightly increases with the amplitude. The minimum stiffness value was found to be equal to the stiffness of a ring beam having the same coil diameter and a cross section moment of inertia equivalent to full slip between the wires. The displacement amplitude corresponding to the minimum effective stiffness was empirically expressed as a function of the coil diameter and a weak function of the wire rope diameter. The stiffness–amplitude relationship was found by fitting the normalised data points.

The energy dissipation/amplitude relationship showed that the damping mechanism is a combination of a friction damping and a rate-independent linear damping. Equating the energy dissipated by the combined mechanism to that dissipated by viscous damping, an expression for the equivalent viscous damping ratio as a function of the displacement amplitude was developed. This expression was fitted to the damping-amplitude relationship.

Appendix. Notation

List of symbols

a_g	acceleration due to gravity
$C_{ED1,2}$	fitting constants for amplitude-dependent dissipated energy
$C_{\theta 1,2}$	constants in the expression for free vibration rotation of the SDOF system
D_c	coil diameter
d_r	wire rope diameter
E	modulus of elasticity
E_D	dissipated energy per vibration cycle
E_D^f	dissipated energy per free vibration cycle
E_D^{fV}	energy dissipated per free vibration cycle by viscous damping
E_D^{hV}	energy dissipated per harmonic vibration cycle by viscous damping
$E_S^{\max}$	maximum strain energy stored in the wire rope spring
F_f	friction force
F_r	spring restoring force
h	distance between the spring/damper (or wire rope spring) attachment point and pivot point
I_p	pendulum mass moment of inertia about the pivot point
I_{xx}	cross section moment of inertia about the axis of bending
k^{fs}	stiffness of the ring beam under a point load, based on a full slip condition
$k^{\min}$	minimum effective stiffness of a wire rope spring
k^{ns}	stiffness of the ring beam under a point load, based on no slip condition
k^{ps}	stiffness of the ring beam under a point load, based on a partial slip condition
k_r	stiffness of the ring beam under a point load
k_{wr}	effective stiffness of the wire rope spring
k_p^θ	pendulum rotational stiffness
k_t^θ	total rotational stiffness
k_{wr}^θ	effective wire rope spring rotational stiffness
m_p	pendulum mass
n_c	number of coils
T_D	damped natural period of vibration, based on a full cycle
T_{DC}	half of the damped natural period of vibration, based on a compression half-cycle
T_{DT}	half of the damped natural period of vibration, based on a tension half-cycle
t	time
X_C	displacement amplitude in compression
X_r	representative displacement amplitude
X_T	displacement amplitude in tension
$X_r^{\min}$	representative displacement amplitude corresponding to minimum wire rope spring stiffness
x	displacement
β	damping ratio (% of critical)
β_{wr}	equivalent damping ratio of wire rope spring (% of critical)
η	dimensionless damping constant
Θ	rotation amplitude
θ	rotation
ω	circular frequency
ω_D	natural damped circular frequency of rotational SDOF
ω_n	natural circular frequency

Operators

•	Differential with respect to time.

Abbreviations

IWRC	independent wire rope core
SDOF	single-degree of freedom
WSC	wire strand core

References

[1] Bouc R. Forced vibrations of a mechanical system with hysteresis. In: Proceedings of 4th conference on non-linear oscillation. 1967, p. 315.

[2] Wen YK. Method for random vibration of hysteretic systems. Journal of Engineering Mechanics Division, ASCE 1976;102:249–63.

[3] Cutchins MA, Cochran JE, Guest S, Fitz-Coy NG, Tinker ML. An investigation of the damping phenomena in wire rope isolators. In: Proceedings of the 1987 ASME design technology conference. 1987, p. 197–204.

[4] Lo HR, Hammond JK, Sainsbury MG. Non-linear system identification and modelling with application to an isolator with hysteresis. In: Proceeding of the 6th international modal analysis conference, vol. 2. 1988, p. 1453–59.

[5] Tinker ML, Cutchins MA. Damping phenomena in a wire rope vibration isolation system. Journal of Sound and Vibration 1992;157: 7–18.

[6] Ko JM, Ni YQ, Tian QL. Hysteretic behaviour and empirical modelling of wire-cable vibration isolator. International Journal of Analytical and Experimental Modal Analysis 1992;7:111–27.

[7] Demetriades GF, Constantinou MC, Reinhorn AM. Study of wire rope systems for seismic protection of equipment in buildings. Engineering Structures 1993;15:321–34.

[8] Tinker ML, Cutchins MA. Instabilities in a non-linear model of a passive damper. Journal of Sound and Vibration 1994;176:415–28.

[9] Ni YQ, Ko JM, Wong CW. Mathematical hysteresis models and their application to non-linear isolation systems. In: Proceedings of the 6th international conference on recent advances in structural dynamics, vol. 2. 1997, p. 1043–57.

[10] Ni YQ, Ko JM, Wong CW, Zhan S. Modeling and identification of a wire-cable isolator via a cyclic loading test, Part 1: Experimental and model development. Journal of Systems and Control Engineering 1999;213.

[11] Ni YQ, Ko JM, Wong CW, Zhan S. Modeling and identification of a wire-cable isolator via a cyclic loading test, Part 2: Identification and response prediction. Journal of Systems and Control Engineering 1999;213.

[12] Ni YQ, Ko JM, Wong CW. Non-parametric identification of non-linear hysteretic systems. Journal of the Engineering Mechanics, ASCE 1999;125:206–15.

[13] Wang JY, Ni YQ, Ko JM. Transient dynamic response of Preisach hysteretic systems. In: Proceedings of the international workshop on seismic isolation, energy dissipation and control of structures. 1999.

[14] Chopra AK. Dynamics of structures. Upper Saddle River (NJ): Prentice Hall; 1995.

[15] Den Hartog JP. Strength of materials. 1st ed. New York: Dover Publications Inc.; 1961.

[16] Connor JJ. Introduction to structural motion control. Massachusetts Institute of Technology, Online version. 1999.